Single-Chip Two Antennas for MM-Wave Self-Powering and Implantable Biomedical Devices

D. Elshaekh [1], S. Kayed [2], and H. Shawkey [3]

[1] Electrical Dept., Faculty of Engineering-Badr University, Badr University in Cairo
dalia-mohamed@buc.edu.eg

[2] Head of Electrical Dept., Obour High Institute for Engineering and Technology, 31 Elasmalia - Desert Road
dr.somayaismail@ohie.edu.eg

[3] Microelectronics Dept., Electronics Research Institute, 12622, El Dokki, Giza, Egypt
heba_shawkey@eri.sci.eg

Abstract ─ Implantable biomedical applications arise the need for multi-band sensors with a wideband frequency channel for RF energy harvesting operation. Using a separate antenna for energy harvesting can simplify device circuit complexity and reduces operation frequency bands interference. This paper demonstrates the design of single chip with two separate integrated antennas for implantable biomedical applications. The two antennas have different structures with orthogonal polarization to achieve low mutual coupling and negligible interaction between them. The first antenna is a multi-band meander line (MBML) designed for multiple channels data communication, with quad operating bands in the MM-wave range from 22-64 GHz with area $1150 \times 200\mu m^2$. The second antenna is a wideband dipole antenna (WBDA) for RF energy harvesting, operates in the frequency range extend from 28 GHz to 36 GHz with area $1300\times250\mu m^2$. The proposed antennas are designed by using high frequency structure simulator (HFSS) and fabricated by using UMC180nm CMOS technology with total area 0.55 mm2. The MBML frequency bands operating bandwidths can reach 2 GHz at impedance bandwidth ≤ -10 dB. While, the WBDA antenna has gain -2 dB over the operating band extend from 28 GHz up to 36 GHz. The antenna performance is simulated separately and using the human-body phantom model that describes layers of fats inside body, and shows their compatibility for in body operation. Die measurements is performed using on wafer-probing RF PICOBROBES and shows the matching between simulation and measurement values.

Index Terms ─ Implantable antenna, Multi-Band Meander-Line (MBML), on-chip antenna, radio frequency energy harvesting and UMC 180 µm CMOS, Wideband Dipole Antenna (WBDA).

I. INTRODUCTION

Currently, promising implantable systems have been proposed for healthcare monitoring and remote sensing to improve the lifestyle of the patients. UWB frequency bands are applied for implantable devices as it enables high data rate and multiple frequency channels for multimode operation [1-5]. Recently, MMW range is described as a complementary imaging technique instead of exposure of patient to radiations as magnetic resonance, X-Ray or Ultrasound [6-8]. The antennas depend on 5G technology to meet the capacity, latency and the bandwidth requirements to support the request of the growing number of wireless communication users [9-10]. Besides, antenna and associated electronics could be designed to support multiple frequency channels for data communications of a group of implantable sensors simultaneously, with the need for a wideband frequency channel for RF energy harvesting to obtain a suitable power level for device operation [11-14]. Figure 1 shows the energy/power required for device operation can be obtained using energy harvester/wireless powering transfer from external source to be applied to the implantable devices in different locations in-body. Different types of on-chip implantable antennas are described in the sub GHz range and MMW range [15-20].

Simultaneous data communication mode and RF wireless powering mode using same antenna and matching network [21-22] where the antenna toggles between the two communication modes, the data mode and power mode, but this needs special control technique to fulfil continuous switching between both modes. To reduce circuit complexity, the modes of operation can be split up by using two separate antennas, one is used for data communication (for multiple sensors) while the other operates for RF energy harvesting. In this paper,

Submitted On: March 13, 2021
Accepted On: June 5, 2021

https://doi.org/10.47037/2021.ACES.J.360710

two separate integrated antennas on the same chip are proposed to be used for self-powering implantable biomedical devices. The antennas are designed for data communication and energy harvesting simultaneously, with two different structures are designed, a multiband meander line antenna (MBML) and a wide-band dipole antenna (WBDA), with no radiation coupling occurs. The MBML resonates at the 22, 36, 48, 60 GHz, such that it is suitable for multiple sensing applications, while the WBDA operates from 28 GHz-36 GHz to perform the wideband required for energy harvesting. The 3D configuration of the proposed antennas shown in Fig. 2, is fabricated using UMC 0.18µm CMOS technology with 6-Metal layers. As implantable devices are affected by the permittivity of human tissues which causes signal losses, antenna design should consider the human-body effect during antenna design as wireless transfer between the on-body device and the external electronic circuits. For human activity monitoring, the implant is set to be below the human scalp or embedded in the muscle [23].

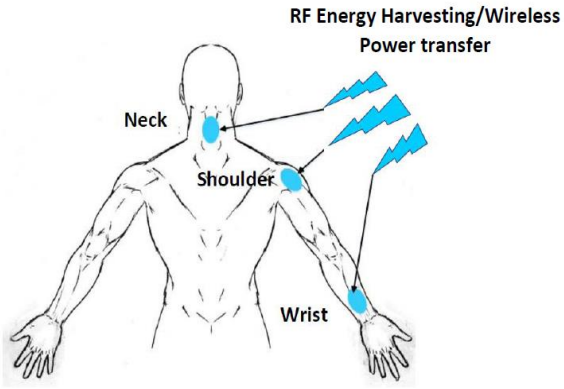

Fig. 1. RF wireless powering for different implantable devices.

In this paper, the chip is assumed for implantation in the fat layer of the human body. Phantom model is used to investigate the antenna signal transmission in the human body layers even in the presence of perturbations such as embedded muscle layers and blood vessels. Different sensor antenna are implemented in a chip 180 nm CMOS technology for radio frequency (RF) energy harvesting to increase the lifetime of the internal batteries or feed another system [30].

The paper sections are organized as follows; Section 2 shows detailed explanation of the proposed antennas configuration. In Section 3 the simulation and measurement performance of both antennas. In Section 4, the proposed antenna simulation using human-phantom is performed to investigate antenna compatibility with implantable applications. Finally, conclusions of the paper are shown in Section 5.

II. ANTENNA CONFIGURATION AND DESIGN

Different shapes of on-chip integrated antennas are shown, as dipole [17], [24], [25], loop [18-20], zigzag [26], [27], and bowtie antennas [28], [29]. This is due to their circuits have differential input / output. The design of the two balanced antennas are utilized to obtain the benefits of the on-chip ground plane used to improve antenna radiation efficiency. Two different shapes of antennas are used to seeking different wireless applications, one for the data communication antenna and the second for wireless powering antenna integrated on the same chip with separate connecting PADS as shown in Fig. 3. The polarization of both antenna are linear polarized and there are orthogonal located to each other to reduced coupling between them. The chip is fabricated by using UMC 180nm CMOS process with silicon substrate and six metal layers. In this section, design and simulation for each antenna is demonstrated.

A. Data communication antenna

It is a multi-band meander line (MBML) implemented at 2 stacked layers to increase antenna total length-located at metal layers M6 and M4 as shown in Fig. 3. A layer of metal M1 is set as a ground plane to enlarge bandwidth with area of 1525µm × 250µm with four connections to the four ground PADS. Each meander layer – whether at M_4 and M_6 – has a finger line width 15µm, length 1150µm and line spacing 20µm between each two fingers. The meander structure at M_6 layer has five fingers while the meander structure at M_4 layer has only four fingers as shown in Fig. 2. The two layers have the same alignment but shifted 17.5µm, to increase number of resonance frequency bands. Five PADS are used with area 80µm×60µm for each and separated by 150µm. One of the PADs is connected tom the upper meander layer M6 to be used as signal PAD and the others are used as ground PADs. The MBML has a 50ohm line connection with signal PAD. The two meander layers are connected through via 1.

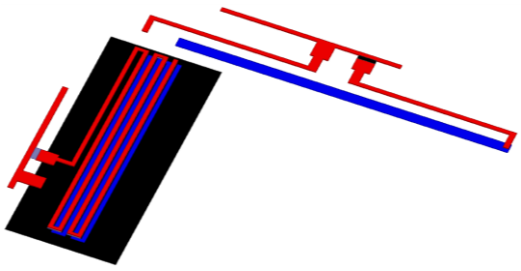

Fig. 2. The 3D configuration of MIMO.

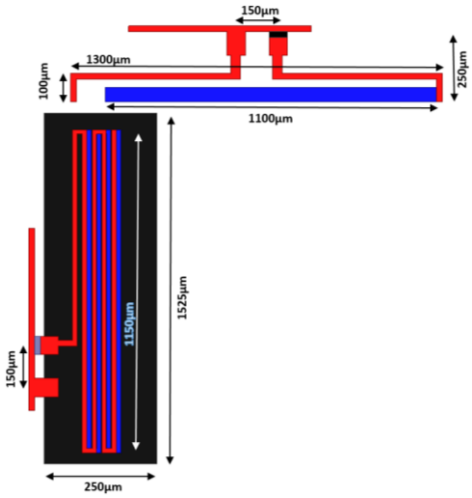

Fig. 3. Data communication of system muti-band meander line and dipole antenna.

B. RF energy harvester antenna

Figure 3 shows the structure of the wideband dipole antenna used for RF energy harvesting. It is composed of three layers, a dipole layer, a patch layer, and a ground plane. The dipole consisting of a half wavelength radiating dipole implemented at the upper metal layer M_6 with total area 1300µm×250µm. The patch layer is carried out in the intermediate metal layer M_4 with area 1100µm×50µm. This middle patch layer acts as a parasitic element to broaden the antenna bandwidth. A ground layer is set at the M_1 layer with area 1300µm×250µm. The patch layer is stacked to the dipole by VIA1. The signal and ground PADs (with area 80µm×60µm) are separated by 150µm. The ground M_1 layer is connected to the Ground PAD by VIA2. The proposed dipole antenna with patch layer is set to reduce the resonant frequency and increase the antenna bandwidth. The corresponding reflection coefficient response for both antennas is shown in Fig. 4 (a), where $|S_{22}|$ (as dashed blue line) represents the MBML response while $|S_{11}|$ (as black line) represents the WBDA. The green line explains the neglected coupling between both antennas. Current distribution at different tuning frequencies on both antennas' surfaces are shown in Fig. 5. The highest magnitude of current represents the corresponding element of radiation.

III. ANTENNA MEASUREMENTS RESULTS

The measured antenna S-parameters are carried out by using cascade probe station on top with Anritsu Vector Network as shown in Fig. 6. The measured reflection coefficient is achieved by using on-wafer probing. The measurements setup shown in Fig. 6, composed of one GSG 70 GHz PicoProbe-RF probe (pitch: 150 µm) and Anritsu Vector Network analyzer up to 70 GHz. The UMC180nm setup die (miniasic 1.525 mm × 1.525 mm) is fabricated and fixed at PM5 KarlSuss manual probe-station.

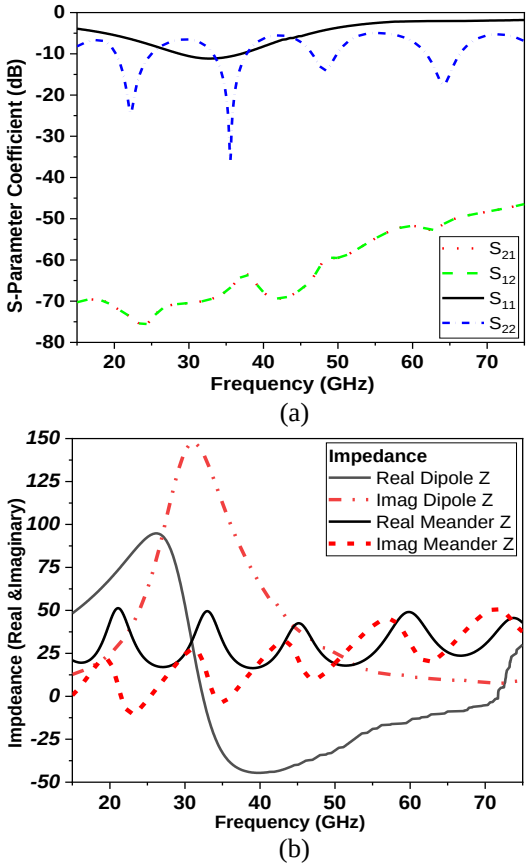

Fig. 4. (a) Scattering parameters versus frequency of the proposed antennas, and (b) input impedance real and imaginary.

The fabricated photo of the proposed antennas are shown in Fig. 6 with four ground PADS connected to the ground metal layer M_1, the extra PADS have no effect on antenna performance but are added due to measurements concerns. To ensure the reliability and accuracy of measurements; the proper fixture is applied. The die is fixed on the probe-station holder using vacuum pump while the GSG probe and the positioner are held by a manipulator that has magnetic fixture to ensure accurate contact between the die and the GSG probe. The other measurement problems that could be cause uncertainty of measurements [29] which is avoided by using a calibration substrate at the beginning of the measurements to ensure accurate calibration for the complete setup (network analyzer, cabling and probe) whenever it produces a reading different than the standard. Besides, before each measurement experiment the VNA was calibrated using (the open short, through calibration kit). Figure 7 (a) shows the comparison between the simulated and measured reflection coefficients $|S_{11}|$ of the double

meander antenna. However, the $|S_{11}|$ of the different dipole length is shown in Fig. 7 (b). The comparison between simulated and measured results showed that there are a good agreement between the lower and the upper of the operating frequencies' antenna bands. There are some ripples in the measured results and there are about −3 dB shift in the measured reflection coefficient results. These errors could be attributed to metal holder, which are not considered and many factors as the thickness of the layer, metal holder was not considered. In addition, uncertainty in the dielectric material properties are specified up to 15 GHz while the simulated dielectric material properties of the layer were identified up to 70 GHz. As well as the influence of larger wafer with the chuck and the uncertainty in the dielectric material properties. In the simulations, these values have been used for the characterization of the structure at 70 GHz. Table 1 shows the radiation pattern of the MBMA at different resonant frequencies. While table 2 shows the simulated polar radiation pattern for the WBDA antenna at three resonant frequencies 28 GHz, 32 GHz and 32 GHz, respectively.

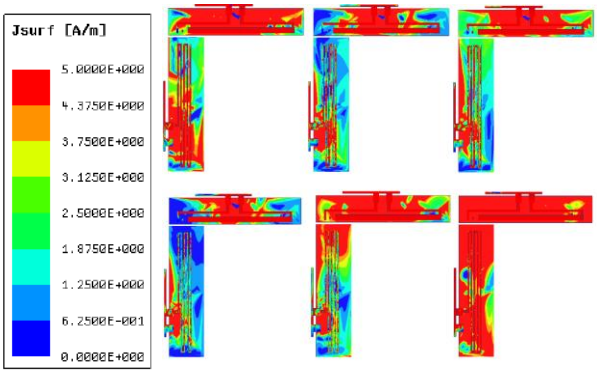

Fig. 5. Current distribution of the two antennas at different tuning frequency: (a) 22 GHz, (b) 28 GHz, (c) 30GHz, (d) 34 GHz, (e) 44 GHz, and (e) 62 GHz.

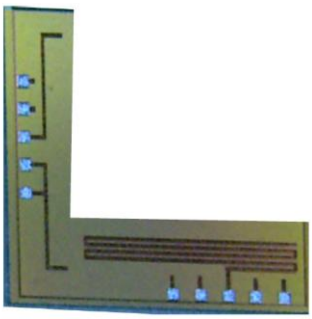

(a)

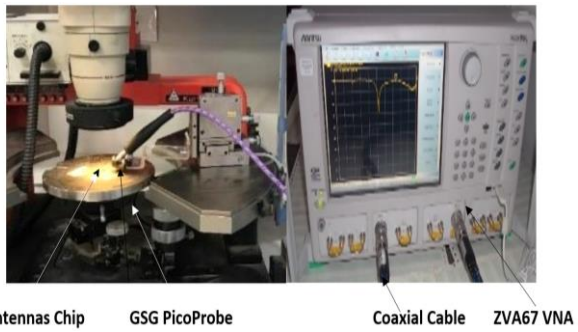

(b)

Fig. 6. (a) Photo of the fabricated antennas, and (b) the reflection coefficient measurement setup.

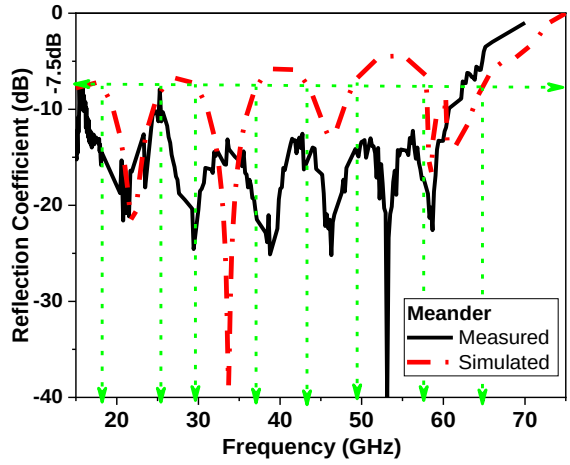

(a)

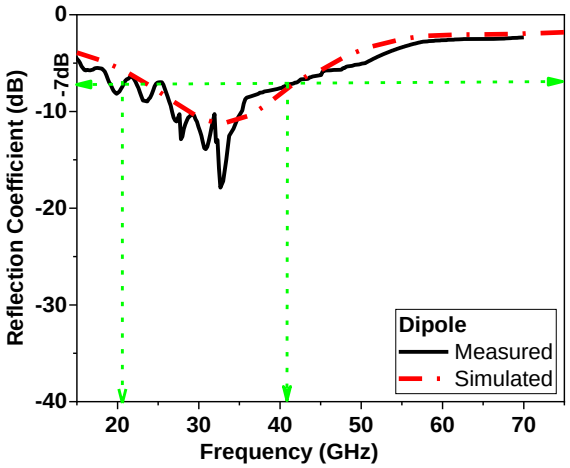

(b)

Fig. 7. Comparison of the proposed antennas measured and simulated of $|S_{11}|$: (a) DBMA and (b) WBDA antenna.

Table 1: The 2D polar radiation pattern ━ without human-body, - · - with human-body at different resonant frequencies

Plane	22 GHz	34 GHz	45 GHz	58 GHz
φ=0°	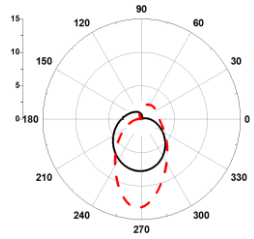	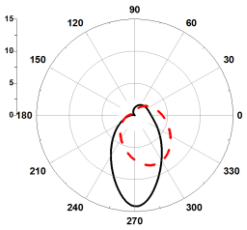	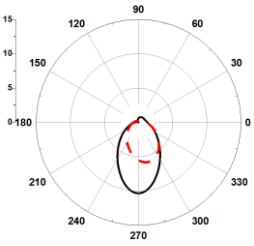	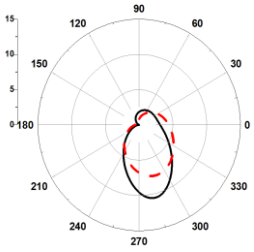
Θ=90⁰	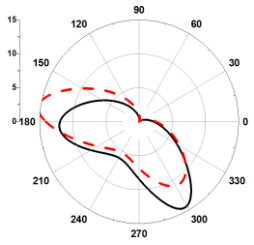	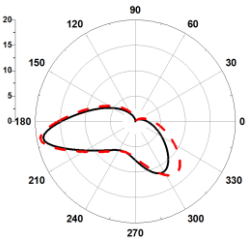	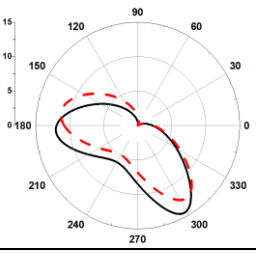	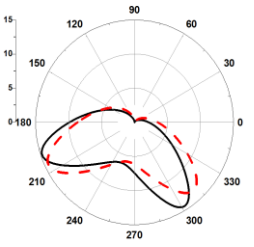

Table 2: THE 2D polar radiation pattern ━ Φ=0⁰, - · - Φ =90⁰, and - ·· - θ =90⁰ at different resonant frequencies

28 GHz	30 GHz	32 GHz
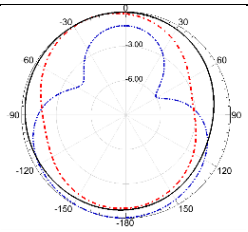	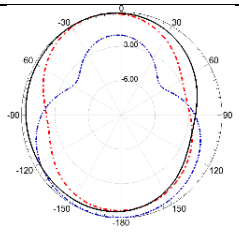	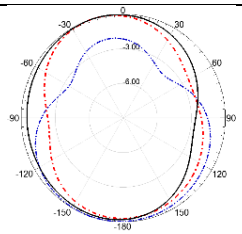

IV. HUMAN-BODY PHANTOM MODELING

To validate the performance of the proposed antennas for implantable applications, phantom model is used to simulate the implanted antenna and evaluate its performance to be used in-body environment. The specific absorption rate (SAR) is important factor that show that if these antennas are safe or not on the human body. SAR factor depend of the electrical field radiation and conductivity of the human tissues. According to IEEE standard it should be the SAR over 1g and 10 g of tissue of less than 1.6W/Kg and 2 W/Kg, respectively. Figure 8 shows the homogeneous multilayered model with a dimension of 80 × 40 × 63 mm^3 used to model human tissue [30]. The values of electrical properties are tuned around 40 GHz, the implanted depth in skin layer is 2 mm. inside the human body. The resonant frequencies are reduced and the operating bandwidths are broaden. The results as shown in Fig. 9 for both proposed antennas showed that when the human body effect is included in the simulation, the antenna impedance matching is more significant for the chip implanted. Moreover, the phase of the reflection coefficient was slightly changed when the chip is placed outside a human body, and it was abruptly changed when the antenna was implanted in the human body. The changed results of the antenna performance are due to the conductivity of the human body, which adds extra load on the antenna surface and changes in the electrical properties of the substrate. However, when the chip is implanted in the human body, it became more dispersive and the operating bandwidths at −10dB (VSWR ≤ 2) were extended from 20 GHz to 45 GHz and from 57 GHz up to 65 GHz as shown in Fig. 9. However, in both simulation scenarios, the antenna bandwidth still operated in the selected bands of operations. The packaging proposed antenna are done by light-weight polymer-based materials that are biocompatible, RF-transparent, easy-to-process, and low-cost. On the other side the embedded antennas have a peak broadside power density of −60 dBW/m^2 at a distance of 1 m. For an isotropic radiator with a transmit power of 1 W, the power density at a distance of 1 m is equal to −11 $dB\ W/m^2$, and for the embedded patch with a gain of −50 dB the power density would be equal to −61 $dB\ W/m^2$.

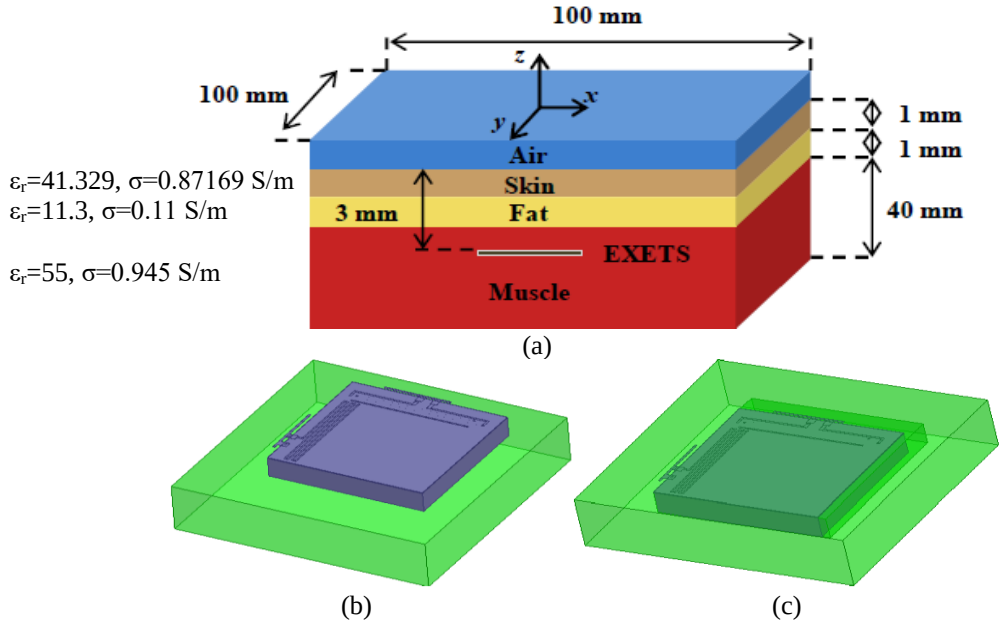

Fig. 8. (a) Simulation model of proposed antennas system, (b) outside the human phantom, and (c) inside the human phantom.

Table 3: Comparison of the proposed antenna with other on-chip antennas

Ref.	**[15]**	**[16]**	**[17]**	**[18]**	**[19]**	**[20]**	**This work**
Type	Dipole		Spiral Slot	Loop	Loop	Loop	Meander/Dipole
Freq	915 MHz	24/60 GHz	0.9 Ghz	60 Ghz	434 MHz	67GHz	22/ 34/ 44/58GHz. 26-34 GHz
Gain	-56 dB	-9/-1dB	-90dB	-3.2 dBi	16.45 dB	8dBi	-20/-15/-10/-1dBi
BW	26MHz	180/700MHZ	53%	5.5GHz	--	4GHz	5/6/4/8GHz
Area	2.52 mm^2	0.794 mm^2	0.385 mm^2	2.25 mm^2	2.56 mm^2	0.875mm^2	0.55 mm^2
Tech.	0.13µm CMOS	0.13µm CMOS	0.18 µm CMOS	0.18 µm CMOS	0.18 µm CMOS	0.18-µm CMOS	0.18-µm CMOS

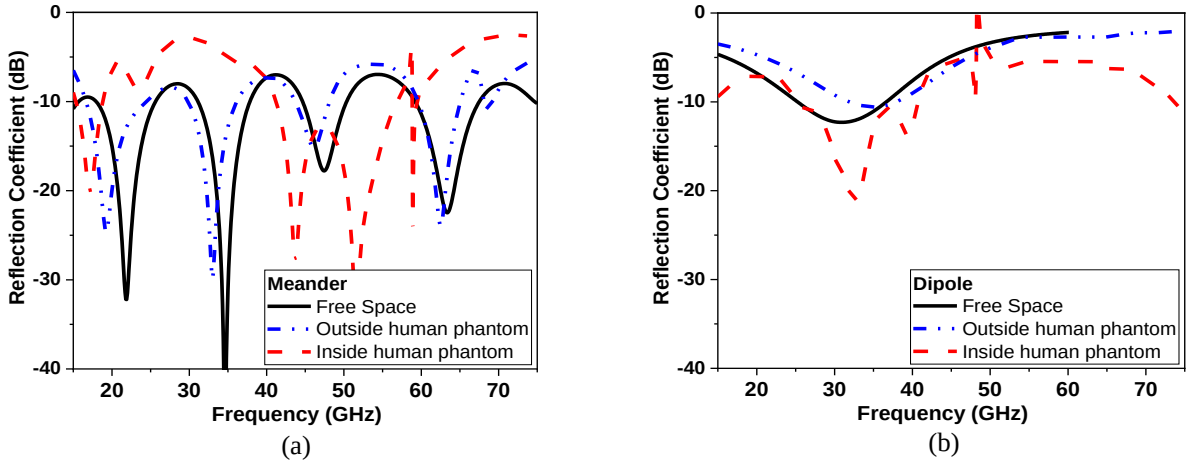

Fig. 9. Reflection coefficient versus frequency: (a) of the meander antenna and (b) of the dipole antenna.

The main drawback of such antennas design is the short communication range, which makes very hard reading process for the patient. As well as it is effect on the radiation efficiency due to the strong coupling of the near field components to the encapsulation of the antenna and electromagnetic absorption in the body tissues [30]. Which it could not to maintain a continuous communication link between the capsule and the external receiver. Table 3 tabulates different types of CMOS antennas operated at different frequencies; at high frequencies the gain is almost about -2 dB.

VI. CONCLUSION

This paper described two antennas integrated on the same- chip for implantable biomedical applications. Two separate antennas are designed with orthogonal polarization to ensure neglected mutual coupling between them. The first antenna (MBML) is used for data communication with multiple resonance frequencies at 22 GHz, 34 GHz, 44 GHz and 62 GHz.

The other antenna (WBDA) has a wideband from 28 GHz up to 36 GHz and used for RF Energy Harvesting. The antennas are fabricated using UMC 180nm CMOS technology with total area 0.55 mm2. Measurements for both antennas - gain and bandwidth - are matched with design and simulation results. The proposed antennas are simulated using phantom model to check their compatibility for implantable devices.

REFERENCES

[1] D. Elsheakh, H. Shawkey, and S.Saleh, "A 9 - 10.6 GHz microstrip antenna-UWB low noise with differential noise canceling technique for IoT applications," *Int. Journal of Communications, Network and System Sciences*, vol. 12, pp. 189, 2019.

[2] R. Elyassi and G. Moradi, "Flexible and moon-shaped slot UWB implantable antenna design for head implants," *International Journal of Microwave and Wireless Technologies*, vol. 9, pp. 1559-1567, 2017.

[3] A. Priya, S. K. Mohideen, and P. Thirumaraiselvanm, "Propagation losses of UWB antenna for on-body to in-body Signal Propagation," *Progress in Electromagnetics Research M*, vol. 73, pp. 101-109, 2018.

[4] H. Shawkey and S. Saleh, "Low-power fully monolithic MICS band receiver for 402-405 MHz implantable devices," *International Journal of Electronics*, vol. 107, no. 1, pp. 28-45, 2020.

[5] H. Shawkey and D. Elsheakh, "Multiband dual-meander line antenna for body-centric networks biomedical applications by using UMC 180 nm," *Electronics*, vol. 9, 1350, 2020.

[6] T. Wu, T. S. Rappaport, and C. M. Collins, "The human body and millimeter-wave wireless communication systems: Interactions and implications," *IEEE International Conference on Communications (ICC)*, 2015.

[7] M. Ali, H. Shawkey, A. Zekry, and M. Sawan, "One Mbps 1 nJ/b 3.5–4 GHz fully integrated FM-UWB transmitter for WBAN applications," *IEEE Trans. Circuits Syst. I: Regul*, vol. 65, pp. 2005-2014, 2018.

[8] C. Liu, Y. Guo, X. Liu, and S. Xiao "An integrated on-chip implantable antenna in 0.18μm CMOS technology for biomedical applications," *IEEE Transactions on Antennas and Propagation*, vol. 64, no. 3, Mar. 2016.

[9] F. Gutierrez, Jr., S. Agarwal, K. Parrish, and T. S. Rappaport, "On-chip integrated antenna structures in CMOS for 60 GHz WPAN systems," *IEEE Journal on Selected Areas in Communications*, vol. 27, no. 8, Oct. 2009.

[10] R. Yuwono and I. Mujahidin, "Rectifier using UWB microstrip antenna as electromagnetic energy harvester for GSM, CCTV and Wi-Fi transmitter," *Journal of Communications*, vol. 14, no. 11, Nov. 2019.

[11] K. Celik and E. Kurt, "A novel super wideband circular fractal antenna for energy harvesting applications," *International Symposium on Advanced Electrical and Communication Technologies (ISAECT)*, 2019.

[12] M. G. Tampouratzis, D. Vouyioukas, D. Stratakis, and T. Yioultsis "Use ultra-wideband discone rectenna for broadband RF energy harvesting applications," *Technologies Journal (MDPI)*, 2020.

[13] V. Kuhn, C. Lahuec, F. Seguin, and C. Person, "A multi-band stacked RF energy harvester with RF-to-DC efficiency up to 84%," *IEEE Transaction on Microwave Theory and Techniques*, vol. 63, no. 5, May 2015.

[14] J. Huang, J. Wu, Y. Chiou, and C. Jou, "A 24/60 GHz dual-band millimeter-wave on-chip monopole antenna fabricated with a 0.13-mCMOS technology," *In Proceedings of the IEEE International Workshop on Antenna Technology*, Santa Monica, CA, USA, Mar. 2-4, 2009.

[15] A. A. Masius and Y. C. Wong, "On-chip miniaturized antenna in CMOS technology for biomedical implant," *International Journal of Electronics and Communications*, vol. 115, Feb. 2020.

[16] Y, Song, Q. Xu, Y. Tian, J. Yang, Y. Wu, X. Tang, and K. Kang, "An on chip frequency-reconfigurable antenna for Q-band broadband applications," *IEEE Antennas Wireless Propagation Letters*, 2017.

[17] H. Rahmani and A. Babakhani, "A dual-mode RF power harvesting system with an on-chip coil in 180-nm SOI CMOS for millimeter-sized

biomedical implants," *IEEE Transactions on Microwave Theory and Techniques*, vol. 67, no. 1, 2018.

[18] Y. Song, Y. Wu, J. Yang, and K. Kang, "The design of a high gain on-chip antenna for SoC application," *Advanced Materials and Processes for RF and THz Applications (IMWS-AMP), 2015 IEEE MTT-S International Microwave Workshop Series on*, Suzhou, pp. 1-3, 2015.

[19] T. D. P. Perera, D. N. K. Jayakody, S. K. Sharma, S. Chatzinotas, and J. Li, "Simultaneous wireless information and power transfer (SWIPT): Recent advances and future challenges," *IEEE Communications Surveys & Tutorials*, vol. 20, no. 1, 2018.

[20] X. Peng and J. Li, "Harvested energy maximization of SWIPT system with popularity cache scheme in dense small cell networks," *Hindawi Wireless Communications and Mobile Computing*, vol. 2019.

[21] J. M. Felício, C. A. Fernandes, and J. R. Costa, "Wideband implantable antenna for body-area high data rate impulse radio communication," *IEEE Transactions on Antennas and Propagation*, vol. 64, no. 5, May 2016.

[22] I. El Masri, T. L. Gouguec, P. Martin, R. Allanic, and C. Quendo, "Integrated dipole antennas and propagation channel on silicon in Ka band for WiNoC applications," *IEEE 22nd Workshop on Signal and Power Integrity (SPI)*, May 2018.

[23] M. Nafe, A. Syed, and A. Shamim, "Gain-enhanced on-chip folded dipole antenna utilizing artificial magnetic conductor at 94 GHz," *IEEE Antennas and Wireless Propagation Letters*, vol. 16, Sep. 2017.

[24] R. S. Narde, J. Venkataraman, A. Ganguly, and I. Puchades, "Antenna arrays as millimeter-wave wireless interconnects in multi-chip systems," *IEEE Antennas and Wireless Propagation Letters*, vol. 19, no. 11, Nov. 2020.

[25] R. S. Narde, N. Mansoor, A. Gangul, and J. Venkataraman, "On-chip antennas for inter-chip wireless interconnections: Challenges and opportunities," *12th European Conference on Antennas and Propagation (EuCAP)*, Apr. 2018.

[26] M. S. Khan, F. A. Tahir, and H. M. Cheema, "Design of bowtie-slot on-chip antenna backed with E-shaped FSS at 94 GHz," *10th European Conference on Antennas and Propagation*, June 2016.

[27] S. Pan, L. Gilreath, P. Heydari, and F. Capolino, "An on-chip W-band bowtie slot antenna in silicon," *Proceedings of the 2012 IEEE Int. Symposium on Antennas and Propagation*, Nov. 2012.

[28] M. R. Karim, X. Yang, and M. F. Shafique, "On chip antenna measurement: A survey of challenges and recent trends," in *IEEE Access*, vol. 6, pp. 20320-20333, 2018.

[29] Y. Zhang, C. Liu, X. Liu, and K. Zhang, "A miniaturized circularly polarized implantable RFID antenna for biomedical applications," *International Journal of RF and Microwave Computer Aided Engineering*, Wiley Periodicals, Inc., Dec. 2019.

[30] M. Caselli, M. Ronchi, and A. Boni, "Power management circuits for low-power RF energy harvesters," *Journal of Low Power Electronics and Applications*, vol. 10, no. 29, pp. 1-17, 2020.

Dalia M. Elsheakh received the B.Sc., M.Sc. and Ph.D. degrees from Ain Shams University in 1998, 2005 and 2010, respectively. M.S. Thesis is on the Design of Microstrip PIFA for Mobile Handsets. Ph.D. Thesis is in Electromagnetic Band-Gap Structure. From 2010 to 2015, she was Assistant Prof. and from 2016 until 2019 she is Associate Prof. in Microstrip Dept., Electronics Research Institute. From 2019 until now she is the Head of Electronics and Communication Program in Faculty of Engineering and Technology, Badr University in Cairo. She was Assistant Researcher at Hawaii Center for advanced Communication (HCAC), College of Engineering, Hawaii University, USA at 2008 and Assistant Prof. at 2014 and 2018. Elsheakh has authored/co-authored four chapters in books. She has published 59 papers in peer-refereed journals and 50 papers in International Conferences. She is a member in many contracted projects (13 research and development project) funded from many funding agencies such as ASRT, NTRA, NSF, STDF, etc. She has three patents. She is an IEEE senior member from 2019.

Somaya I. Kayed is an Associate Professor and Head of the Electrical Dept. (Electronics, Communication, Computer and Control Engineering) at Oubor Higher Institute for Engineering and Technology. She graduated in 1987 from Ain Shams University with a B.Sc. in Electronics and Communications Department, with general grade (very Good). She finished her Masters of Science (M.Sc.) and Ph.D. from Ain Shams University at 1995 and 2000 respectively. She was an Acting Dean for the 2019 first term at Oubor Higher Institute for Engineering and Technology. Her related research interests (Analog

and digital VLSI design, current conveyor, nano-electronics).

Heba A. Shawkey received her B.Sc. and M.Sc. in Electrical Engineering, in 1993 and 2000, respectively, with honor degree from Ain Shams University-Egypt and her Ph.D. degree in 2005 from the Cairo University-Egypt. Heba has been working in Electronics Research Institute since 1994 and her main research interests are wireless communication systems design, analog/mixed-signal/RF circuits, especially high speed PLL and frequency synthesizers. She also has many publications in low power digital circuit design, biomedical sensors read-out circuits, interconnect modeling and low power networks on chip (NoC). Now Heba is a member in nanotechnology lab and working in the field of nanomaterial electronics applications as graphene and CNT.